CHAPTER 8

STRUCTURAL DESIGN AND ANALYSIS OF 6-DOF CYLINDRICAL ROBOTIC MANIPULATORS FOR AUTOMATED AGRICULTURE

JORDAN KURIAN KURUVILLA[1], ATIRAV SETH[1], JYOTISHKA DUTTAGUPTA[2], SHASHWAT SHARMA[2], and ANKUR JAISWAL[1]

[1]*Department of Mechatronics, Manipal Institute of Technology, Manipal Academy of Higher Education (MAHE), Manipal, Karnataka, India*

[2]*Department of Mechanical and Manufacturing Engineering, Manipal Institute of Technology, Manipal Academy of Higher Education (MAHE), Manipal, Karnataka, India*

ABSTRACT

Research has been conducted on static industrial cylindrical manipulators used in controlled environments such as factories that generally use steel or aluminum for construction. This paper compares the performance of different engineering materials under various loading conditions when designing a cylindrical robotic manipulator for use in the automated precision agriculture industry. The 6-DOF cylindrical robotic arm is designed for automated agriculture in varied terrain found in farmlands. The manipulator requires high specific stiffness, and its structure must be resistant to collisions. The

Precision Agriculture for Sustainability: Use of Smart Sensors, Actuators, and Decision Support Systems. Narendra Khatri, PhD, Postdoc, Ajay Kumar Vyas, PhD, Celestine Iwendi, PhD & Prasenjit Chatterjee,PhD (Eds.)

design of the arm has been analyzed with forces such as the impact of the forward collision rather than payload and inertial loads, which are the usual requirements from robotic arms. A comprehensive analysis of the structures compares the performance of various materials such as prepreg carbon fiber, aluminum 6061-T6, and steel 1045 using finite element method (FEM). Agricultural vehicles on which the arm is mounted may have to cross bund walls with slopes with gradients of up to 60°. As a result, the vector for collision forces may vary. As a result, simulations are carried out on the arm in different loading directions. Results of FEM simulations changing the materials and loading direction are compared, and the material that takes the required load while being cost-effective for agricultural purposes is determined.

8.1 INTRODUCTION

Robotic manipulators with multiple degrees of freedom find applications in various domains such as medicine,[13] fabrication,[22] warehouse management,[12] and material handling. Increased dependence on robotic manipulators to achieve high levels of automation has fueled further research into their applications in novel domains.

Refinement and improvement of the mechanical design of robotic manipulators have been centered around workspace, redundant configurations, accuracy, repeatability, speed, rigidity, strength, weight, and singularity avoidance. This research explores the application of multi-DOF robotic manipulators with a cylindrical coordinate system-based workspace on autonomous, off-road, and extraterrestrial exploration vehicles referred to as unmanned ground vehicles (UGV). UGVs may be utilized to automate predictable tasks requiring a mobile operation. UGVs can be outfitted with specialized suspensions[3] and robotic arms[23] to introduce terrain traversal and object manipulation capabilities, respectively. Industries such as agriculture present immense scope of implementing such technologies to reduce human labor.

The structure of the robotic arm is designed to meet the following parameters:

1. Payload capacity at end effector = 5 kg.
2. Horizontal reach from the base of the arm = 800 mm.
3. Vertical reach range = 1255 mm above and 610 mm below the mounting surface.
4. 270° swivel base range of motion.

8.2 LITERATURE REVIEW

In Ref. [1], Fikrul Akbar Alamsyah shows how to fuse filament fabrication (FFF) 3D printing can be carried out using an RPP-type 3-DOF cylindrical manipulator. To model the cylindrical arm as an FFF 3D printer, reference frames are established using the D-H approach to tackle kinematics in simulation.

Albani in Ref. [2] describes a system of swarm robots for agricultural purposes. UAVs are used for monitoring and mapping weed in a field.

Billing et al.[4] outline the development of NASA-JPL's Curiosity Rover's ruggedized robotic arm, whose end-effector houses five turret-mounted scientific analysis instruments weighing 37 kg in total. The arm weighs 67 kg and can withstand severe temperature ranges and high inertial loads experienced during landing and traversal.

Victor Bloch in Ref. [5] discusses three different configurations of a 3-degree of freedom manipulator (RRR, PRR, and PPP) and compares them for optimal harvesting of apples in an orchid.

In Ref. [6], Rishabh Chaturvedi develops three robotic arm designs composed of three different engineering materials, AISI-1050 Steel, carbon fiber, and kevlar29. Static, modular, and fatigue analyses are performed on all the variants to determine the most reliable structure and material.

The authors in Ref. [7] use ANSYS 17.0 ACP to compare the performance of pressure vessels made from filament wound carbon, glass, and Kevlar fibers in an epoxy matrix.

Yasuhiko Ishigure in Ref. [8] proposes a design for a pruning robot that uses self-weight and a power-saving chainsaw drive. The bot can stay on a tree without consuming any energy since it uses its weight to support itself.

Kannan et al. employ ANSYS Workbench 18.0 AC Pre and Post to analyze and improve the design of a hybrid aluminum-prepreg carbon fiber and epoxy composite drive shaft in Ref. [9].

Narayan et al.[14] utilize CAD and CAE to iterate the design of a five-degree-of-freedom manipulator with a three-jaw gripper for use in physical rehabilitation therapy.

To compare constructions, detect failure points, and perform topology optimization to conserve material, Sai Santosh in Ref. [19] uses ANSYS workbench to perform finite element analysis on ABS and PLA.

Oberti in Ref. [15] proposes a 6-DOF arm with a precision spraying actuator and an optical sensor. This arm is designed for automatic detection

and selective spraying of grapevine canopy areas exhibiting symptoms of powdery mildew.

In Ref. [16], Ali Roshanianfard presents a design for a 4-degree of freedom robotic manipulator that can be used for harvesting heavy crops such as melons and pumpkins. This robotic arm is designed as an actuating unit of a robot tractor for the outdoor agricultural environment.

The authors in Ref. [17] utilize industry-grade software, Solidworks, and ANSYS workbench for the iterative design of a 3-DOF robotic manipulator. The manipulator is explicitly designed to enhance structural rigidity and accuracy and used in robotic biopsy and tissue extraction procedures.

Philip J. Sammons proposes a design[18] for an autonomous four-wheel pesticide spraying robot for use in a greenhouse.

In Ref. [20], Shanmugasundar et al. demonstrate a comprehensive set of design processes to be followed for the construction of a robotic manipulator. The authors use topological optimization tools on FEM software (ANSYS Workbench) to improve the specific stiffness of the design.

The authors in Ref. [23] describe the instrument deployment device (IDD) design, which is the 5-DOF manipulator outfitted on NASA's twin geological survey rovers, Spirit and Opportunity. The manipulator exhibits high repeatability and is equipped with a 2-kg science payload at its end effector, containing four in situ analysis instruments.

Wang studies all configurational permutations of 6-DOF manipulators that only have turning and sliding pairs and obtains the Cartesian, cylindrical, spherical, articulated, and double cylindrical robotic arm configurations in Ref. [24].

Zhang et al.[25] investigate the kinematics, dynamics, and FEA-based design of a 3-DOF manipulator with two translational and one rotational degrees of freedom for pick-and-place operations in postprocessing parts produced by powder metallurgical manufacturing.

8.3 CONFIGURATION

The cylindrical robotic arm uses a cylindrical coordinate system. It can be designed in three main serial configurations, which pertain to the order of the DOF's in the robotic manipulator: PPR, PRP, and RPP.[25] For the design of this robotic manipulator, the PRP configuration has been utilized. The vertical reach requirements of the arm necessitate a vertical prismatic joint with a range of motion of 1255 mm. Consequently, the vertical prismatic

joint structure is bulky, consisting of three guide rods arranged in a triangular formation. Hence, it is advantageous to provide fixed support at the base of the vertical prismatic joint. It also reduces the load on the revolute joint as it is located serially after the prismatic joint. Although it can be argued that a suitable floating assembly at the base revolute joint can be used to delocalize the stress in the RPP configuration, the additional weight of such an assembly far outweighs its advantages pertaining to our application. This configuration also enables the use of guy wires to provide additional rigidity to the first prismatic structure. This is possible since the guy wires would not get entangled, which would have been the case with the RPP configuration.

While the workspace offered by the PRP configuration is lower than the RPP configuration for the same horizontal reach from the base, the smaller radial arm increases accuracy at the end effector, as shown by the formula below:

$$\delta l = R \times \delta\theta$$

δl being the arc motion at the end of a radial arm of radius R, due to an angular mechanical play of $\delta\theta$.

Although the PPR configuration offers many of the same benefits as the PRP type, the constricted workspace is a significant disadvantage for the intended application.

8.4 ADVANTAGES

Compared to articulated, SCARA-type, and delta configuration manipulators, the cylindrical manipulator has various advantages:

- End effector motion along individual axes can be controlled individually due to two prismatic joints in the cylindrical arm. Tasks that require the end effector to follow a straight line, for example, are simple to complete, such as the sowing of seeings, harvesting, and installing fencing. The use of multiple rotating joints in articulated and SCARA-type arms results in the end effector position changing along two axes at once, making the arm more challenging to control.
- The SCARA configuration requires bulky revolute joints to minimize structural deflection since the two revolute joints are loaded perpendicular to the plane of rotation. On the other hand, the cylindrical arm has a horizontal prismatic joint as its third DOF. The horizontal

prismatic joint structure offers a more excellent strength-to-weight ratio for vertical loading.
- The delta manipulator configuration requires an overhead mounting surface, which is not practical due to the excess weight of the mounting bracket.
- Delta manipulators have a lower payload capacity and structural rigidity due to design constraints of the actuation links.
- The articulated configuration has a large radial arm that amplifies the error due to $l = R \times \delta\theta$. Inverse/Forward kinematics is required to achieve straight line motion, which is a major advantage in agricultural applications, as mentioned above.

8.5 COMPONENTS OF THE MANIPULATOR

The manipulator is divided into the robotic arm and the end effector, comprising 3 DOFs each. The robotic arm discussed in this paper is of PRP configuration, consisting of two translational DOFs and one rotational DOF for positioning the manipulator. The end effector consists of 2 rotational DOFs for orientation and a single DOF of the gripping mechanism. The translational joints are prismatic joints actuated by lead screw and timing belt mechanisms.

8.5.1 1ST PRISMATIC JOINT

FIGURE 8.1 1st prismatic joint.

Since the manipulator configuration is PRP, the first prismatic is used to mount the manipulator to the robot's chassis or any mounting surface.

The guide rod structure, which is the main structural component of the cylindrical manipulator, consists of three roll-wrapped carbon fiber tubes of custom dimensions to ensure maximum rigidity while ensuring low weight. These tubes are mounted in a triangular pattern, which provides an adequate second moment of area for collision forces in the horizontal plane. The tubes are mounted using aluminum 6061-T6 CNC milled connector blocks bolted to the mounting surface. The mounting blocks were topology optimized based on FEM analysis on ANSYS Workbench 19.2. The two larger hind tubes have an outer diameter of 63 mm and a thickness of 1.5 mm, and the smaller aft tube has an outer diameter of 30 mm and a thickness of 2.5 mm. The aft tube is smaller in diameter to prevent hindrance to the revolute joint to swivel a complete 250 degrees and to felicitate using a commercial ball-circuit linear bearing (three tubes).

A lead screw mechanism actuates the first prismatic. Its nonback drivability (at our specified loading and lead screw specifications) lets us use a lighter motor to power the leadscrew since the holding torque requirement reduces significantly. Hence, a motor of a lower-rated torque can be adequately utilized. The total deformation values of the first prismatic in all loading and collision cases were maintained within 2 mm, preventing buckling of the leadscrew, resulting in binding of the screw pair. This ensures no damage to the lead screw mechanism in terms of wear and tear, even if the collision occurs while the lead screw mechanism is being actuated.

Bearing assemblies on the top and bottom mounting plates also ensure that negligible axial and bending loads are transferred to the lead screw motor, ensuring extended life of the motor.

Reinforcement guy wire bracings provide additional rigidity to the first prismatic structure. The guy wires are attached from the top plate to the mounting surface, and turnbuckles adjust the tension. The wires used are 3 mm 6 × 7 steel wire ropes. The guy wires provide an exceptionally high strength-to-weight ratio since they are under tensile loading. The commercially available guy wires have very high load ratings for relatively small diameter or mass of the wire, which ensures that the rigidity of the structure is improved drastically while keeping the additional weight negligible.

The carbon fiber tubes were analyzed using ANSYS composites pre/post, wherein AC pre is utilized to set up the carbon fiber tube fiber orientation and shell parameters. The AC post is used to study the failure theory values such

as the Tsai-Wu and Tsai-Hill constants for composite or anisotropic materials.

8.5.2 CARRIAGE

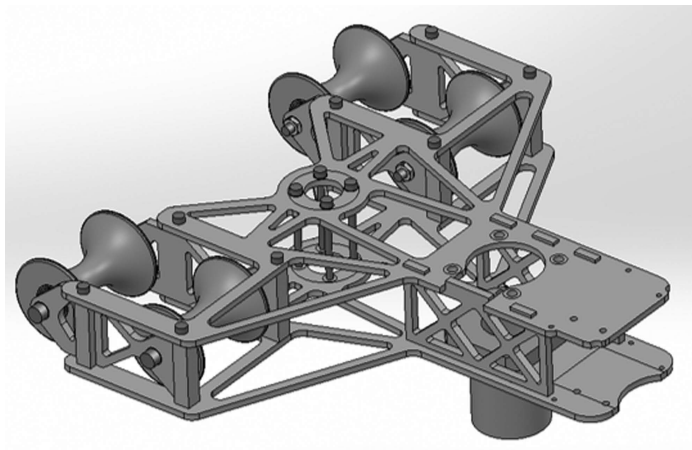

FIGURE 8.2 Carriage.

The carriage is the gantry assembly actuated by the lead screw mechanism in the first prismatic joint. It is a space frame structure consisting of aluminum 6061-T6 topology-optimized top and bottom plates that are bolter together with spacer plates oriented vertically to have a lightweight yet rigid space frame assembly.

CNC turned nylon arc-contact rollers are constrained onto the tubes by the space frame structure to ensure that the carriage distributes the load on the tubes evenly. These rollers are used for the hind tubes instead of linear bearings to reduce the total weight of the assembly since commercially available ball-cycle Linear bearings for this scale of tubes weigh more than 2 kg. The rollers are fitted with deep groove ball bearings, which support the rollers on shafts fixed to the carriage.

The carriage top and bottom plates sandwich the swivel gearbox between them, ensuring that the mounting is secure and the load distribution is even. Two lead nuts have been utilized, one mounted on each of the top and bottom plates, ensuring that both the plates have equal load distribution of the actuation forces. Each roller has a 130° contact arc with the cylindrical tubes, thus giving 260° of total arc contact to maximize load distribution.

The rollers aid in distributing the remote loads and collision forces evenly on the tubes to avoid any high-stress points on the carriage structure or tubes.

8.5.3 REVOLUTE JOINT

The Revolute joint in the manipulator connects the overhang and the first prismatic carriage. The revolute joint is driven by a Worm and Worm wheel gearbox, which has a 40:1 reduction ratio, which is actuated by a geared DC motor. The gearbox is intrinsically nonback drivable, which helps self-lock the revolute joint when the motor is unpowered. The worm gearbox contains the bearing assembly for the revolute joint, and the gearbox casing is structurally analyzed for taking collision and loading forces.

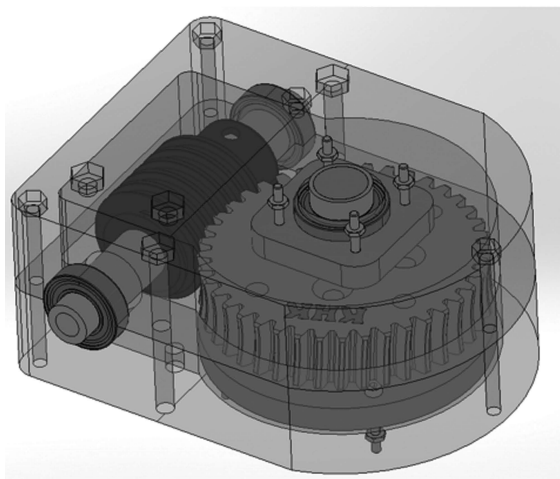

FIGURE 8.3 Revolute joint.

The gearbox's output is given by a four-bolt mounting, which axially runs through all gearbox parts, ensuring that the load is distributed evenly throughout the assembly. The worm gear shaft has a fully constrained bearing assembly that features two inner race and two outer race abutments, efficiently delocalizing the stress into the gearbox casing through the deep-groove ball bearings. The gearbox casing can be manufactured by CNC milling a nylon billet or commonly available FDM 3D printing using Nylon filament material.

8.5.4 OVERHANG STRUCTURES

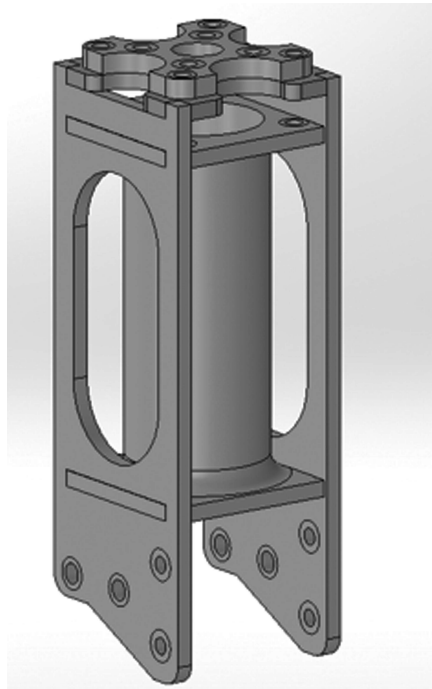

FIGURE 8.4 Overhang structure.

The overhang is a structural part of the arm used to mate the gearbox to the second prismatic structure. Such a structure was required to provide vertical travel of the end effector below the level of the mounting surface, which would be an essential feature for agricultural applications. It makes use of a system consisting of AL 6061-T6 plates and a central tubular structure, which is AL 6063. The structure was iteratively designed to take frontal impact and torsional loads, where the initial designs were based on AL 6061-T6 plates, with the eventual addition of tubes. The aluminum plates on the sides of the structure are used to dissipate the frontal bending loads. It can do this effectively by virtue of its high second moment of area. As the arm experiences torsional loads in addition to frontal bending, a hollow aluminum tube was also included to manage the stresses that arrive from such loading effectively. FEA was performed on these parts, and their topology was optimized.

8.5.5 2ND PRISMATIC JOINT

FIGURE 8.5 2nd prismatic joint.

The second prismatic's structural member is a 4040 cross-section Aluminum T-slot extrusion. Like what is seen on an FDM 3D printer, the setup consists of a carriage actuated by a timing belt drive. The carriage is constrained to the extrusion by POM pulley wheels placed on all four sides, ensuring the carriage's stability and smooth translation along the T-slot extrusion. Eccentric nuts are used to optimally adjust the clearance between the T-slot and the pulley wheels by enabling the height of the bolts to be varied, thereby allowing us to prevent wobble. The timing belt pulley used is tensioned using a movable pulley constrained using T-nuts. By varying the extension/retraction of the tensioner, the belt tension can be optimally adjusted. The carriage was designed using a similar design philosophy as the overhang and constructed using Al 6061-T6. The space frame structure is a bolted assembly consisting of CNC milled Al 6061 billets. A combination of plates and tubular structures helps effectively dissipate stresses associated with the loads the second prismatic carriage may experience since the end effector is mounted to it.

8.5.6 END EFFECTOR

The end effector is the manipulator component. Having 3 degrees of freedom gives precision control to the operator. The end effector features a bevel gear

differential that provides degrees of freedom of pitch and roll. The gripper uses a 4-bar slider-crank mechanism, actuated by a lead screw, which helps achieve an encompassing grip. The gripper has been designed to pick up as big as 40 cm × 40 cm × 40 cm. The gripper's jaws are lined with compliant 3D-printed gripping pads that can easily be switched with a cutting tool that may find application in agriculture.

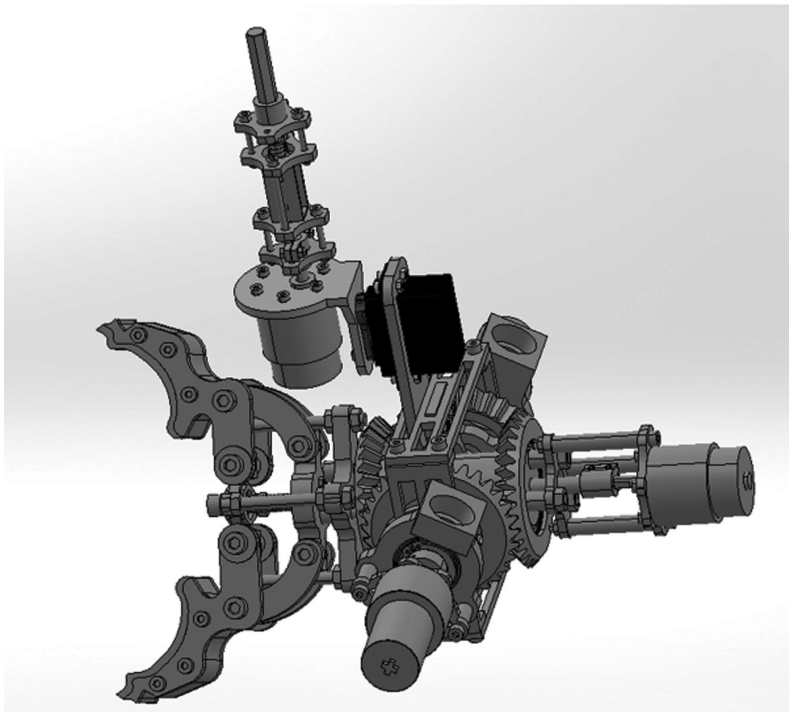

FIGURE 8.6 End effector.

8.6 STRUCTURAL ANALYSIS

8.6.1 MATERIAL SPECIFICATION

ANSYS Workbench 19.2 was used for the finite element simulations of the structures used in the robotic manipulator. The material properties of the materials that were utilized for the FEM analysis-aluminum 6061-T6, steel 1045, carbon fiber woven Prepreg (390 GPa), and stainless steel 304 are as follows:

TABLE 8.1 Material Specifications.

Material	Density (kg m^3)	Tensile yield strength (MPa)	Poisson's ratio	Young's modulus (GPa)
Steel 1045	7870	310	0.29	200
Aluminum 6061-T6	2770	280	0.33	68
Carbon fiber	1480	829 (X and Y)	0.3	91.8
Stainless steel	7850	250	0.3	190

8.6.2 LOADING CONDITIONS

The collision cases in agricultural robots, such as the cylindrical manipulator mentioned in this paper, include collision with farming equipment, bunds, tree branches, and agricultural vehicles such as tractors and harvesters. Agricultural robots have to face the elements all year round and undergo a lot of wear and tear due to a harsh working environment.

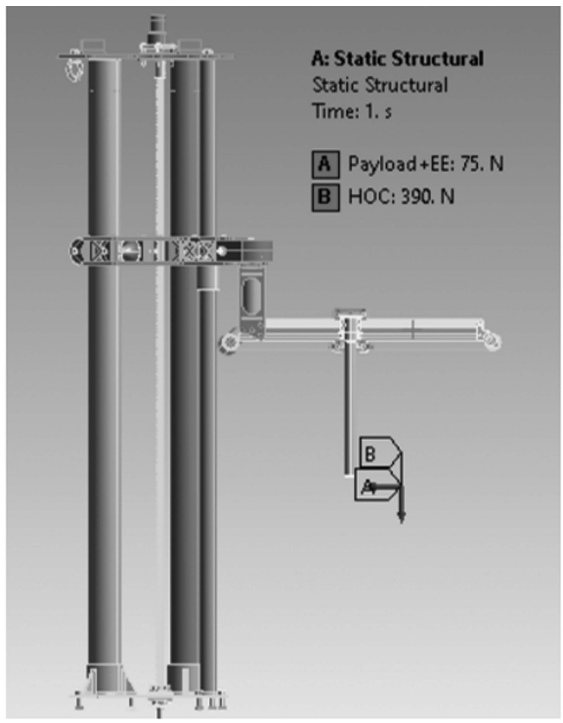

FIGURE 8.7 Loading conditions.

Loading conditions are shown in Figure 8.7. The point of collision is the end effector, which collides into a rigid object at the maximum velocity (V_{max} = 1.6 m/s) of the UGV on which the manipulator is mounted. The two forces, "A," which is the forward collision force, which was calculated to be 390 N, and "B," which signifies the mass load of the end effector (25 N), plus the Payload (50 N), result in a total load of 75 N.

The collisions are not always perfectly normal to the end effector, like tree branches and bunds, for example, are at various angles with respect to the horizontal plane, which results in components of the head-on collision force to result in varied angles of collision. Thus, the simulation's collision angles range from 60° to −60°, which is the average range of the bunds and tree branches found in farmlands.

8.6.3 MESHING

A hexa/prism mesh using a multizone method with a size of 2 mm is used. The multizone mesh has a quadratic element order and four manual sources for mesh uniformity. The guy wires are meshed using the sweep method with quadratic elements, which have 100 elements, and the tubes were meshed using a uniform surface meshing before applying the ply using AC Pre.

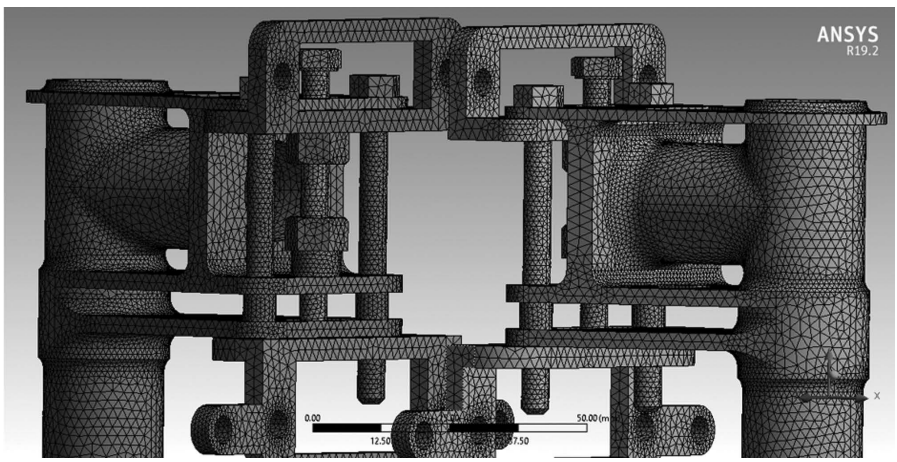

FIGURE 8.8 Meshing.

8.7 RESULTS AND DISCUSSION

8.7.1 1ST PRISMATIC JOINT

TABLE 8.2 Steel 1045.

Angle	Stress	Strain	Deformation
–60°	49.663	0.000594	0.9779
–40°	59.441	0.000611	1.0585
–20°	45.738	0.0005628	1.0236
0°	35.208	0.0004422	0.8615
20°	32.195	0.0002682	0.5996
40°	30.43	0.0001948	0.4078
60°	24.996	0.0001931	0.3403

TABLE 8.3 Aluminum 6061-T6.

Angle	Stress	Strain	Deformation
–60°	71.894	0.00103	2.082
–40°	73.132	0.00103	2.203
–20°	65.549	0.000923	2.0596
0°	50.06	0.000755	1.668
20°	35.668	0.000402	1.0791
40°	33.317	0.000219	0.4679
60°	26.949	0.000307	0.4267

TABLE 8.4 Carbon Fiber.

Angle	Tsai-Wu	Stress	Strain	Deformation
–60°	0.095279	72.569	0.0003656	1.254
–40°	0.096743	73.971	0.0003726	1.3567
–20°	0.086486	66.41	0.000346	1.2962
0°	0.065796	50.839	0.0002561	1.0811
20°	0.03717	29.137	0.00014682	0.7395
40°	0..0055326	8.9826	0.000045186	0.36879
60°	0.02904	21.769	0.00010965	0.30247

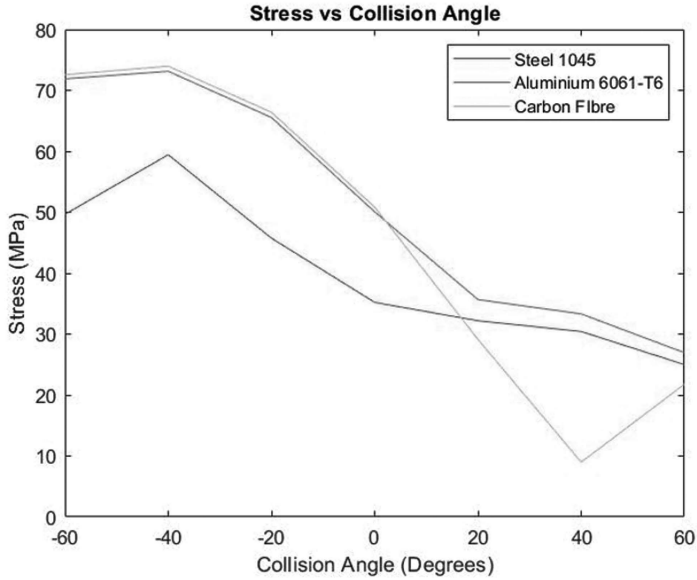

FIGURE 8.9 Stress vs collision angle.

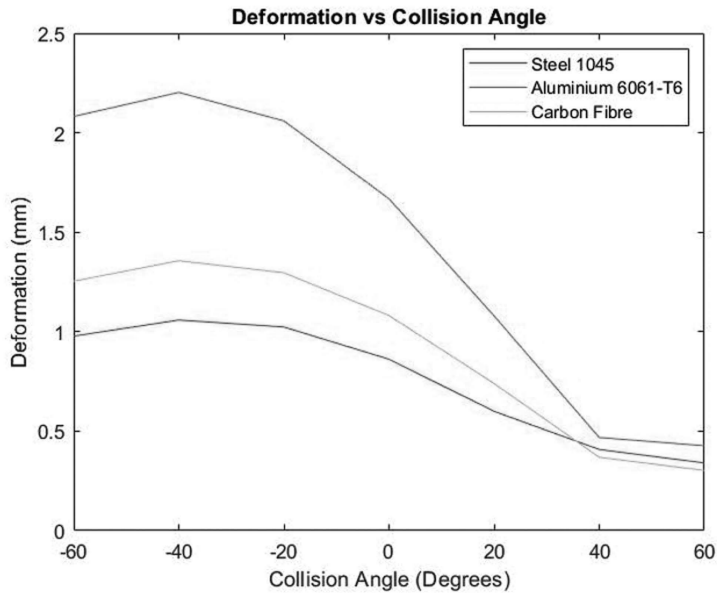

FIGURE 8.10 Deformation vs collision angle.

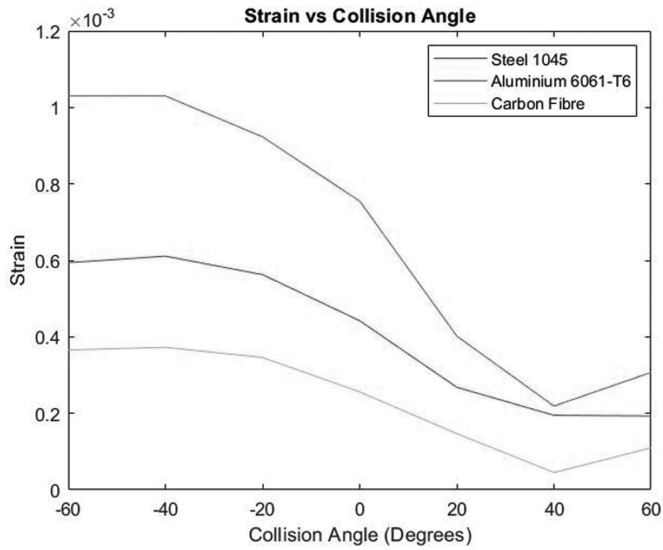

FIGURE 8.11 Strain vs collision angle.

From the above three graphs, it is observed that maximum stress, strain, and deformation for steel 1045, aluminum 6061-T6, and carbon fiber occur at an angle of -40°.

8.7.2 OVERHANG STRUCTURE (I)

The overhang structure (I) is connected directly to the revolute joint output, and it supports the rest of the arm. The maximum deformation is 0.48971 mm (Fig. 8.12), and the maximum stress is 197.31 MPa (Fig. 8.13) at an angle of -40°.

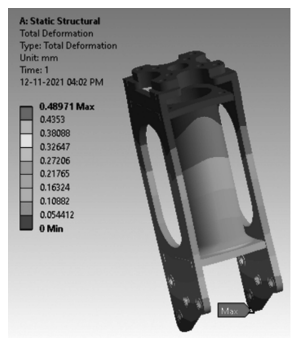

FIGURE 8.12 Overhang maximum deformation.

FIGURE 8.13 Overhang maximum Von-Mises stress.

8.7.3 OVERHANG STRUCTURE (II)

The maximum deformation here is 2.451 mm (Fig. 8.14), and the maximum stress is 193.16 MPa (Fig. 8.15) at an angle of –40°, which is on a part that is milled out of aluminum 7075 alloy.

FIGURE 8.14 Overhang (II) maximum deformation.

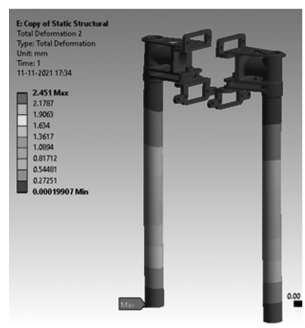

FIGURE 8.15 Overhang maximum von Mises stress.

8.7.4 REVOLUTE JOINT GEARBOX

The Worm gearbox that actuates and supports the revolute joint has a maximum deformation of 0.0463 mm (Fig. 8.16) and maximum stress of 55.667 MPa (Fig. 8.17) at an angle of –40°.

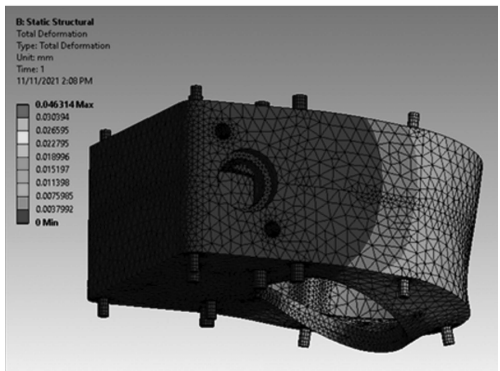

FIGURE 8.16 Worm gearbox maximum deformation.

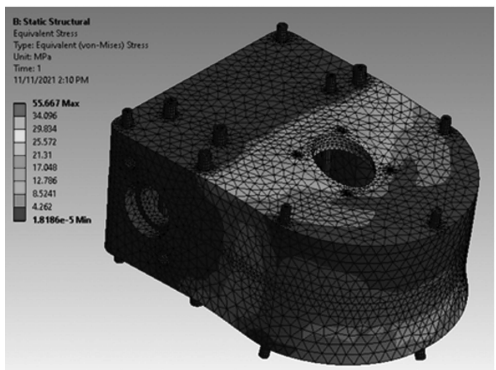

FIGURE 8.17 Worm gearbox maximum Von-Mises stress.

8.8 CONCLUSION

The 6-DOF cylindrical manipulator has been analyzed and simulated through FEM on ANSYS Workbench 19.2 for the various loading conditions discussed earlier, based on collision with various agricultural equipment, trees, and bunds.

The stress vs collision angle graph shows that carbon fiber has very similar stress values as aluminum for a given collision angle. It is also seen that steel experiences the least stress for a given collision angle. Hence, steel would be the ideal choice for the least stress developed. However, it is not preferred due to its considerably higher density than Al 6061 and carbon fiber.

From the graph of deformation vs collision Angle, it is seen that carbon fiber has the slightest deformation for a given collision angle, owing to its high rigidity. Hence, carbon fiber is the ideal choice based on these results. However, it is significantly more expensive compared to Al 6061 and Steel 1045.

Carbon fiber is the following best-performing material with low deformation and low strain. Although it performs satisfactorily, carbon fiber has a very low elasticity, which can fracture suddenly without exhibiting any plastic deformation.

Though aluminum 6061-T6 is the worst performing material among the given materials, we see that its structural integrity is never compromised (stress does not exceed yield strength) at any of the collision angles. aluminum is also relatively light compared to Steel and is more economically viable than carbon fiber. Hence, aluminum is the most suitable for the agricultural robotic manipulator.

Overhang structure (I), overhang structure (II), and gearbox manufactured from aluminum 6061-T6 have been tested under the worst-case scenario of total loading at a collision angle of –40°. Even under these conditions, the maximum stress does not exceed the yield strength of aluminum, with a safety factor of 1.4.

KEYWORDS

- **6-DOF**
- **cylindrical manipulator**
- **agricultural robot**
- **CAD modeling**
- **leadscrew actuation**
- **nonback drivable revolute joint**
- **timing belt**
- **space frame assembly**
- **finite element analysis (FEA)**

REFERENCES

1. Alamsyah, F. A. In *The Kinematics Analysis of Robotic Arm Manipulators Cylindrical Robot RPP Type for FFF 3d Print Using Scilab*, IOP Conference Series: Materials Science and Engineering; IOP Publishing, 2019; vol 494, p 012100.
2. Albani, D.; IJsselmuiden, J.; Haken, R.; Trianni, V. In *Monitoring and Mapping with Robot Swarms for Agricultural Applications*, 2017 14th IEEE International Conference on Advanced Video and Signal Based Surveillance (AVSS); IEEE, 2017; pp 1–6.
3. Barlas, F. Design of a Mars Rover Suspension Mechanism. Master's Thesis, Izmir Institute of Technology, 2004.
4. Billing, R.; Fleischner, R. In *Mars Science Laboratory Robotic Arm*, 14th European Space Mechanisms & Tribology Symposium, Constance, Germany, Sept 2011; pp 28–30.
5. Bloch, V.; Degani, A.; Bechar, A. A Methodology of Orchard Architecture Design for an Optimal Harvesting Robot. *Biosyst. Eng.* **2018,** *166*, 126–137.
6. Chaturvedi, R.; Islam, A.; Sharma, K. Anticipated Investigation of a Cylindrical Robot Arm Utilising Compound Materials. *Eur. J. Mol. Clin. Med.* **2020,** *7* (4), 736–745.
7. Hussain, O. A.; Saad, N. A. A. In *An Investigation of Different Composite on the Performance of Pressure Vessel by Filament Winding*, 2021 12th International Conference on Mechanical and Aerospace Engineering (ICMAE); IEEE, 2021; pp 157–160.
8. Ishigure, Y.; Hirai, K.; Kawasaki, H. In *A Pruning Robot with a Power-Saving Chainsaw Drive*, 2013 IEEE International Conference on Mechatronics and Automation; IEEE, 2013; pp 1223–1228.
9. Kannan, V.; Kannan, V. V.; Pemmasani, S. Design Optimisation of an Epoxy Carbon Prepreg Drive Shaft and Design of a Hybrid Aluminium 6061-t6 Alloy/Epoxy Carbon Prepreg Drive Shaft. *Tech. Rep.* SAE Technical Paper, **2018**.
10. Kiran Bollineni, R.; Menon, S. S.; Udupa, G. Design a Rover and Robotic Arm. *Mater. Today Proc.* **2020,** *24*, 1340–1347.
11. Kulkarni, V.; Sahuji, M. A.; Indrale, M. A.; Patil, M. A.; Gunjal, M. S. Cylindrical Robotic Arm for Multipurpose Operation. **2019,** *5* (3).
12. Kumar, S.; Majumder, A.; Dutta, S.; Raja, R.; Jotawar, S.; Kumar, A.; Soni, M.; Raju, V.; Kundu, O.; Behera, E. H. L.; et al. Design and Develop an Automated Robotic Pick & Stow System for an e-Commerce Warehouse. arXiv preprint arXiv:1703.02340, 2017.
13. Lehman, A.; Tiwari, M. M.; Shah, B.; Farritor, S. M.; Nelson, C. A.; Oleynikov, D. Recent Advances in the Cobrasurge Robotic Manipulator and Dexterous Miniature In Vivo Robotics for Minimally Invasive Surgery. *Proc. Inst. Mech. Eng. C J. Mech. Eng. Sci.* **2010,** *224* (7), 1487–1494.
14. Narayan, J.; Mishra, S.; Jaiswal, G.; Dwivedy, S. K. Novel Design and Kinematic Analysis of a 5-DOFs Robotic Arm with Three-Fingered Gripper for Physical Therapy. *Mater. Today Proc.* **2020,** *28*, 2121–2132.
15. Oberti, R.; Marchi, M.; Tirelli, P.; Calcante, A.; Iriti, M.; Ho˘cevar, M.; Baur, J.; Pfaff, J.; Sch¨utz, C.; Ulbrich, H. Selective Spraying of Grapevine's Diseases by a Modular Agricultural Robot. *J. Agric. Eng.* **2013,** *44*, s2.
16. Roshanianfard, A.; Noguchi, N.; Kamata, T. Design and Performance of a Robotic Arm for Farm Use. *Int. J. Agric. Biol. Eng.* **2019,** *12* (1), 146–158.

17. Roy, A.; Ghosh, T.; Mishra, R.; Kamlesh, S. S. Dynamic FEA Analysis and Optimisation of a Robotic Arm for CT Image-Guided Procedures. *Mater. Today Proc.* **2018,** *5* (9), 19270–19276.
18. Sammons, P. J.; Furukawa, T.; Bulgin, A. In *Autonomous Pesticide Spraying Robot for Use in a Greenhouse*, Australian Conference on Robotics and Automation, 2005; vol 1.
19. Santosh, L. P. S.; Mishra, N.; Mahanta, S. S. A.; Dharmarajan, V.; Varma, S. K.; Shoor, S. Design and Analysis of a Robotic Arm Under Different Loading Conditions Using FEA Simulation. *Mater. Today Proc.* **2021**.
20. Shanmugasundar, G.; Sivaramakrishnan, R.; Meganathan, S.; Balasubramani, S. Structural Optimisation of Five Degrees of Freedom (t-3r-t) Robot Manipulator Using Finite Element Analysis. *Mater. Today Proc.* **2019,** *16*, 1325–1332.
21. Shinde, M. R.; Bhaiswar, V.; Achmare, B. Designing a Suitable Robotic Arm for Loading and Unloading Material on Lathe Machine Using Workspace Simulation Software. *Int. Res. J. Eng. Technol.* **2008,** *3* (1).
22. Singh, P.; Kumar, A.; Vashisth, M. Design a Robotic Arm with Gripper & End Effector for Spot Welding. *Univers. J. Mechan. Eng.* **2013,** *1* (3), 92–97.
23. Trebi-Ollennu, A.; Baumgartner, E. T.; Leger, P. C.; Bonitz, R. G. In *Robotic Arm In-Situ Operations for the Mars Exploration Rovers Surface Mission*, 2005 IEEE International Conference on Systems, Man and Cybernetics; IEEE, 2005; vol 2, pp 1799–1806.
24. Wang, K.; Lien, T. K. Structure Design and Kinematics of a Robot Manipulator. *Robotica* **1988,** *6* (4), 299–309.
25. Zhang, L.; Yan, X.; Zhang, Q. Design and Analysis of 3-DOF Cylindrical Coordinate-Based Manipulator. *Robot. Comput. Integr. Manuf.* **2018,** *52*, 35–45.